Available online at www.sciencedirect.com
ScienceDirect
Catalysis Today 129 (2007) 207–214
CATALYSIS TODAY
www.elsevier.com/locate/cattod

Degradation of dipyrone and its main intermediates by solar AOPs Identification of intermediate products and toxicity assessment

Leónidas A. Pérez-Estrada [a], Sixto Malato [a], Ana Agüera [b,*], Amadeo R. Fernández-Alba [b]

[a] *Plataforma Solar de Almería, CIEMAT, P.O. Box 22, 04200 Tabernas, Almería, Spain*
[b] *Pesticide Residues Group, University of Almería, 04120 Almería, Spain*

Available online 18 September 2007

Abstract

In this study, two solar advanced oxidation processes, heterogeneous photocatalysis with TiO_2 and homogeneous photocatalysis by photo-Fenton, carried out at pilot-plant scale using compound parabolic collectors are proposed for the elimination of dipyrone and its metabolites in water. The two treatments are compared on the basis of their kinetics (parent compound and TOC), formation of degradation products (as determined by ionic chromatography, GC/MS and LC/TOF-MS), and toxicity (as evaluated by *Vibrio fischeri* bacteria). Photo-Fenton was more efficient than TiO_2, but without any relevant difference between the degradation products formed or toxicity. A degradation pathway is proposed, carboxylic acids being the main intermediates prior to mineralisation. Decrease in toxicity during treatment is also shown.

Keywords: Dipyrone; 4-Methylaminoantipyrine; Photo-Fenton; Photocatalysis

1. Introduction

Pharmaceutical active ingredients (PAIs) are used worldwide in large quantities for human and veterinary medicine. Their implication and effect on the environment have, however, remained largely neglected [1]. Recently, the evidence of serious adverse effects on non-target populations (endocrine disruption, development of resistant bacteria) has highlighted the need to monitor and control their presence and persistence in the environment. Studies about the fate and occurrence of pharmaceuticals have shown that one of the main routes by which these compounds reach surface water is sewage treatment plants [2–8]. During conventional biological treatments, many of these compounds and/or their metabolites escape degradation and are released into the environment. PAIs belonging to different therapeutic categories have been detected in effluents and natural water all over the world.

One of the most popular analgesic, antipyretic drugs is dipyrone, also known as Metamizole or Novalgin. Despite its potential side effects, dipyrone is widely used in both pediatric and adult patients because it is a strong analgesic, low-cost, and does not require prescription [9]. Dipyrone is a prodrug which, after oral intake, is spontaneously hydrolyzed into its main metabolite, 4-methylaminoantipyrine (4-MAA) and afterwards into a variety of compounds by enzymatic reactions. These metabolites are not biodegradable and, although little is known about their behaviour and persistence in the environment, they have already been detected in effluents and surface water [2,10] at significantly high concentrations.

The use of solar advanced oxidation processes (AOPs), such as homogeneous photocatalysis by photo-Fenton and heterogeneous photocatalysis with TiO_2, in the treatment of non-biodegradable and/or toxic compounds, was first studied at pilot-plant scale [11] a long time ago. During the last decade, this technology grew in use and in variety of applications [12,13]. In recent years, their application to the degradation of pharmaceuticals has also been reported. Different groups of pharmaceuticals have been treated with this technology and the results show its suitability for antibiotics, anti-inflammatory and analgesic drugs [14–17], for which municipal wastewater plants are not effective.

In this study, two solar advanced oxidation processes carried out at pilot-plant scale are proposed for the elimination of

* Corresponding author. Tel.: +34 950015531; fax: +34 950015531.
E-mail address: aaguera@ual.es (A. Agüera).

0920-5861/$ – see front matter
doi:10.1016/j.cattod.2007.08.008

dipyrone and its metabolites in water. It should be mentioned that these processes have been applied directly to 4-methylaminoantipyrine (4-MAA), since dipyrone is readily hydrolyzed to 4-MAA after dissolving in water for a few minutes [9,17]. The two AOP treatments are compared based on their kinetics, formation of degradation products, and the toxicity during the processes.

2. Materials and methods

2.1. Chemicals

Dipyrone was obtained from Sigma–Aldrich. Ultrapure water from a Milli-Q system (Bedford, MA, USA), methanol analytical grade from Panreac (Barcelona, SP), and sodium hydroxide 50% from J.T. Baker (Deventer, Holland) were used for the chromatographic analyses. Iron sulphate ($FeSO_4{\cdot}7H_2O$) analytical grade and hydrogen peroxide reagent grade (30%, w/v) were from Panreac, titanium dioxide was Degussa P25. All the experiments were performed using demineralised water (conductivity $< 10\ \mu S\ cm^{-1}$, $Cl^- = 0.2$–$0.3\ mg\ L^{-1}$, $SO_4^{-2} = 0.2$–$0.3\ mg\ L^{-1}$, organic carbon $< 0.5\ mg\ L^{-1}$).

2.2. Analytical determinations

Total organic carbon (TOC) was analyzed by direct injection of the samples into a Shimadzu-5050A TOC analyzer, equipped with an ASI5000 autosampler. The samples were first filtered using a Millipore 0.2 μm nylon filter and analyzed as soon as they were taken from the pilot plant. Dipyrone and 4-MAA concentrations (Fig. 1) were monitored by reverse phase liquid-chromatography in an Agilent Technologies 1100 HPLC, equipped with a C-18 column (Synergy 4 Fusion, Phenomenex) and diode array detector (DAD) at 254 nm. Before filtering, samples were quenched with a 1:1 methanol dilution to prevent further degradation. Ammonium concentration was determined by isocratic elution with a Dionex DX-120 ion chromatograph (IC) equipped with a Dionex Ionpac CS12A (4 mm × 250 mm) column. Anion concentrations (NO_3^- and carboxylates) were determined in a gradient program by a Dionex DX-600 IC using a Dionex Ionpac AS11-HC (4 mm × 250 mm) column.

2.3. Sample preparation

Solid-phase extraction was employed for pre-concentration of samples prior to mass spectrometry analysis. Oasis® HLB (hydrophilic–lipophilic balance), which assures good recovery of compounds in a wide range of polarities, was used as the sorbent. The cartridges were placed in a vacuum cube (Supelco VISPRIN), conditioned with 2 mL of methanol and washed with 2 mL of deionised water. After the conditioning step, 20 mL aliquots of the water samples were charged, at a flow rate of approximately $10\ mL\ min^{-1}$. Elution was performed with $2\times$ 2 mL of methanol at $1\ mL\ min^{-1}$. The extracted samples analyzed in the GC–MS were injected as obtained. For LC–TOF-MS analyses, the extracted samples were diluted 1:1 with Ultrapure water from a Milli-Q system, prior to injection.

2.4. Identification of degradation products

GC–MS analyses were performed on an Agilent Technologies 6890 gas chromatograph, equipped with an HP-5MS column (30 m × 0.25 mm i.d. × 0.25 μm), coupled to an MSD 5973 selective mass detector (Agilent Technologies). A split–splitless injector was used under the following conditions: injection volume 5 μL; injector temperature 250 °C. The temperature program was 4 min at 105 °C, 25 °C/min to 180 °C, 5 °C/min to 230 °C, and 30 °C/min to 260 °C. Analyses were performed using electron impact ionization (EI) mode at 70 eV. The spectrometer detector was run in full-scan mode from 50 to 500 amu. The MS interface temperature was set at 280 °C, and the ionization source at 250 °C.

Analyses by liquid chromatography electrospray time-of-flight mass spectrometry (LC–MS(ESI)-TOF), with positive ionization, were performed using an HPLC (Agilent Series 1100) equipped with a 150 mm × 4.6 mm C8 column (Zorbax Eclipse XDB-C8). A and B mobile phases were acetonitrile and water with 0.1% formic acid, respectively. The linear gradient

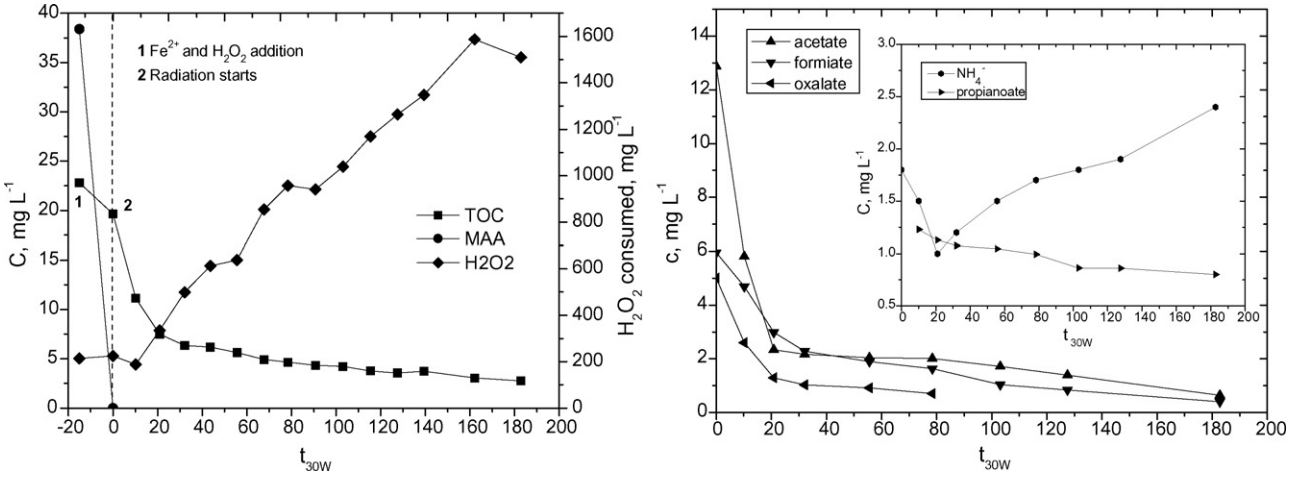

Fig. 1. Photo-Fenton MAA degradation kinetics (left) ($2\ mg\ L^{-1}\ Fe^{2+}$) and evolution of the main carboxylic acids and inorganic species detected (right).

was 15–100% A in 30 min. The flow rate was 0.6 mL/min, and injection volume 50 μL. This HPLC system was connected to an Agilent MSD time-of-flight mass spectrometer with electrospray interface. LC–MS-TOF accurate mass spectra were recorded from 50 to 1000 *m/z*.

2.5. Toxicity evaluation

The toxicity analysis was performed using the BioTox luminometric toxicity test kit with *Vibrio fischeri* bacteria at 5, 15 and 30 min exposure time. The bacteria were purchased from Macherey–Nagen as a freeze-lyophilized reagent, and were stored at −20 °C and activated by hydration with a sterilized solution of sodium chloride prior to the test. Sample pH was adjusted to between 6 and 8 using NaOH or HCl, and adjusting the osmolality of solutions to 2% by adding high-purity sodium chloride. Toxicity was determined as the concentration of a test sample that cause a 50% reduction in the light output measured in a Macherey–Nagen Biofix® illuminometer. All the samples were placed in a thermostatic plate at 15 °C.

2.6. Experimental set-up

Fifty milligrams per litre of dipyrone were prepared in 90 L of demineralised water in a polypropylene tank with an electrical mixer. Then the solar pilot plant was filled for photo-Fenton or TiO_2 photocatalytic treatments. All the experiments were performed in a compound parabolic collector (CPC) solar pilot plant with a total volume of 35 L, illuminated volume of 22 L and irradiated collector surface of 3.08 m^2 [18]. The plant works in batch mode, continuously recirculating the whole volume in the reactor to maintain turbulent flow in the absorber tubes. The temperature inside the reactor is usually between 30 and 40 °C. At the beginning of the experiments, with collectors covered, 35 L of the solution are transferred from the mixing tank to the pilot plant. By that time, dipyrone had already converted to 4-MAA. The pH was adjusted at 2.8, recognized as the optimum value for this process [19]. After that the iron salt and hydrogen peroxide were added. Finally, the cover of the reactor was removed and the photo-Fenton process starts. The samples were collected at predetermined times (*t*). Hydrogen peroxide concentration was maintained around 200–500 mg L^{-1} by continuous addition as it was consumed. For photocatalysis (TiO_2/Solar light), 200 mg L^{-1} of the catalyst (TiO_2) were added before removing the cover. Samples were collected at predetermined times.

Solar ultraviolet radiation (UV) was measured by a global UV radiometer (KIPP&ZONEN, model CUV3), mounted on a platform tilted 37° (the angle of the CPCs), which provides data in terms of incident $WUV^{\bullet}m^{-2}$. This gives an idea of the energy reaching any surface in the same position with regard to the sun. Comparison of the photocatalytic experiments performed on different days is possible using Eq. (1) where t_n is the experimental time for each sample, UV is the average solar ultraviolet radiation measured during Δt_n, and $t_{30\,W}$ is a ''normalized illumination time''. In this case, time refers to a constant solar UV power of 30 W m^2 (typical solar UV power on a perfectly sunny day around noon).

$$t_{30\,W,n} = t_{30} + \Delta t_n \frac{UV}{30}\frac{V_i}{V_T}, \quad \Delta t_n = t_n - t_{n-1}. \tag{1}$$

3. Results and discussion

3.1. Solar photocatalytic treatments

Hydrolysis and photolysis experiments were conducted before the photocatalytic treatments. These studies showed that dipyrone was rapidly hydrolyzed into 4-methylaminoantipiryne (MAA). Once dipyrone had been completely transformed, MAA remained stable for a longer period of time. Due to the absence of mineralisation, pH changes only slightly between pH 5.8 and 6.5. A more detailed study has been published elsewhere [17].

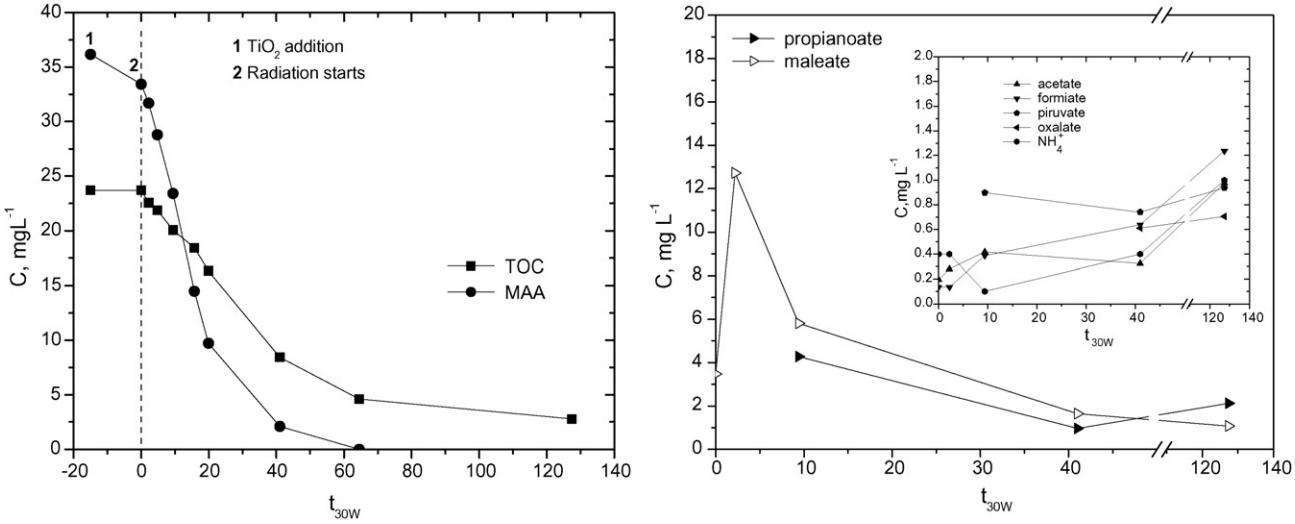

Fig. 2. MAA degradation kinetics (left) during TiO_2 photocatalysis (at 200 mg L^{-1}) and evolution of the main carboxylic acids and inorganic species detected (right).

The photo-Fenton experiments (Fig. 1) were performed using a 2 mg L^{-1} iron concentration. This low concentration of iron was selected after testing at higher concentrations, so degradation intermediates and toxicity would develop more slowly and these parameters could be evaluated more accurately [17]. Complete disappearance of MAA was already observed during the dark Fenton reaction within 15 min after hydrogen peroxide was added. At this point TOC had only decreased by around 10%. Once solar radiation started to enter the reactor, TOC decreased rapidly for the next 30 min of

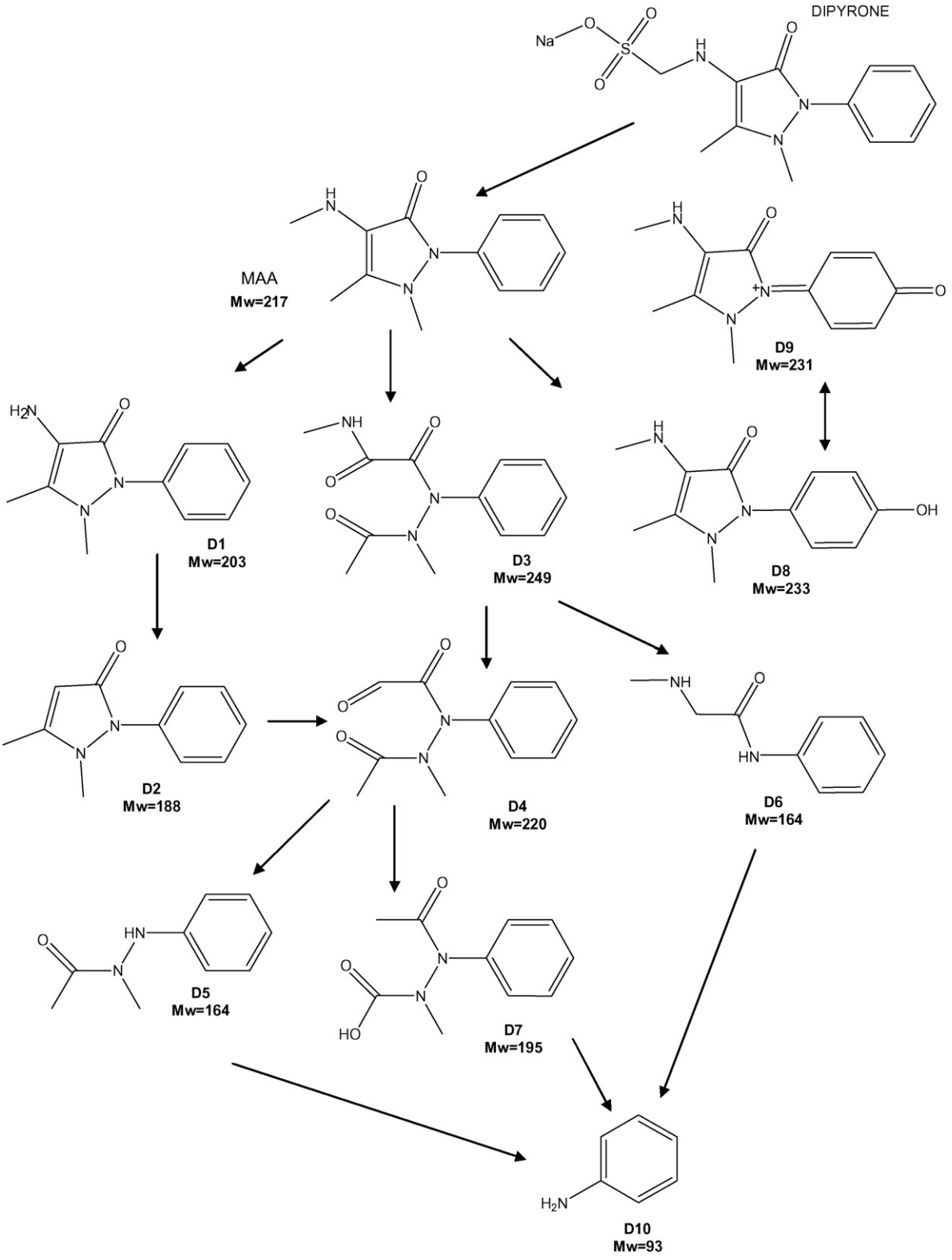

Fig. 3. MAA degradation pathway of during photocatalytic treatment.

treatment, and then up to 60 min, remained at a plateau at around 5 mg L^{-1}, for which 120 min more of solar irradiation were required to reach the final TOC of 2.5 mg L^{-1}. The decrease in TOC took place mainly in two stages, dropping rapidly, from 20 to 5 mg L^{-1} (75% mineralisation) in the first 30 min, and then very slowly, from 5 to 2.5 mg L^{-1} (12.5% mineralisation) in 160 min. The first step could be explained by the mineralisation of the aromatic ring and the three-methyl moieties (responsible for 75% of MAA TOC). The slow second stage is related to the opening and mineralisation of the pyrazole ring. This could be explained by the formation of carboxylic acids described as recalcitrant to the photo-Fenton process [20]. Carboxylic and dicarboxylic acids are known to form stable iron complexes which inhibit the reaction with peroxide. The main carboxylic acids found were acetate, formiate and oxalate at maximum concentrations of 13, 6, and 5 mg L^{-1}, respectively, and some propionate. These compounds were present throughout all degradation, and at a significant concentration at the end of the treatment. The relatively high concentration of these acids at $t_{30\ W} = 0$ min just after the Fenton process (in the dark) shows how weak the MAA molecule is under the attack of the $^{\bullet}$OH radicals, and suggests which bonds the $^{\bullet}$OH radicals attack first. The discussion of the degradation pathway includes more information about this point.

During photocatalysis (Fig. 2), MAA was slightly adsorbed onto TiO_2 (around 5%) and was degraded notoriously more slowly than during the photo-Fenton process. MAA decreased rapidly from 95% to 30%, during the first 20 min of treatment, and completely disappeared after 60 min. The disappearance of MAA followed first-order kinetics ($k = 0.069$ min^{-1}) as usual in heterogeneous photocatalysis (TiO_2). The disappearance of MAA by photo-Fenton occurred very quickly during the first stage in the dark (Fenton reaction), impeding the calculation of degradation kinetics. TOC diminished almost at the same rate as MAA during the first stages, and at a substantially slower mineralisation rate than MAA degradation at the end of the treatment. The carboxylic acids detected at higher concentrations were maleate and propionate at maximum concentrations of 13 and 8 mg L^{-1}, respectively, which formed quickly and degraded more slowly, presumably into lighter-weight carboxylic acids (acetate, formiate, pyruvate and oxalate), which always appeared at very low concentrations during TiO_2 photocatalysis. We suggest that lightweight carboxylic acids, continuously forming and degrading, could not be accumulated at any significant concentration in the treated water during TiO_2 photocatalysis. Therefore, the main carboxylic acids found during the TiO_2 process were different from those determined during photo-Fenton. Indeed, maleate and propionate may be also formed at high concentrations during the first stages of photo-Fenton and rapidly transformed into the lighter carboxylic acids, impeding their detection. Due to formation of small quantities of ammonia pH slightly increased during the first stages of the treatment from pH 5.8 to 7.5, decreasing after due to the formation of carboxylic acids until pH around 4 and increasing again at the end due to organic acids mineralisation.

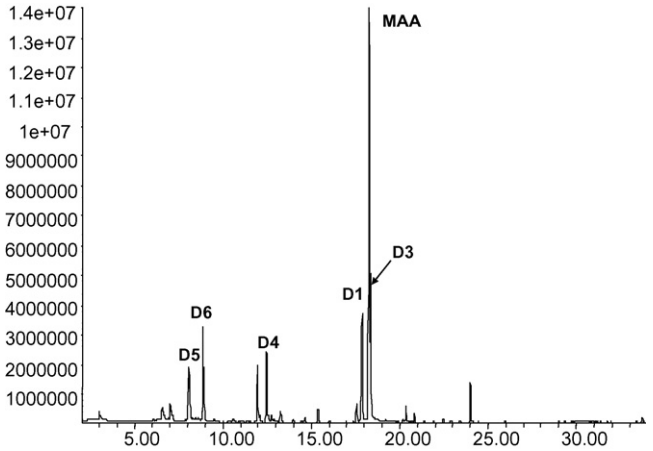

Fig. 4. Typical GC–MS chromatogram of a sample taken after 10 min of TiO_2 photocatalytic treatment.

3.2. Identification of degradation products

The combined use of GC–MS and LC–MS analytical techniques led to the degradation route proposed in Fig. 3.

3.2.1. GC–MS analyses

In addition to MAA, GC/MS analyses led to the identification of five DPs (D1, D3, D4, D5 and D6), which were tentatively assigned by their full-scan mass spectra. Fig. 4 shows a chromatogram of a sample taken after 10 min of TiO_2 photocatalytic treatment. Four of the DPs (D3, D4, D5 and D6), due to opening of the pyrazolinone ring by the $^{\bullet}$OH radical attack on the double bond in the heterocyclic ring, show the same fragmentation pattern with fragments at *m/z* 121, 107, 92 and 77 (see Table 1). Fragment at *m/z* 121 corresponds to the *N*-phenylformamide moiety, present in all these structures. Compounds D3 and D5 have been previously described [21] as trace biotransformation products in human urine. D5 has also

Table 1
Fragment ions, retention times and relative abundances (RA) of MAA and its degradation products determined by GC/MS

Compound	Rt	Mw	Mass fragments (RA, %)
MAA	18.28	217	217 (50), 123 (11), 98 (9), 83 (48), 56 (100)
D1	17.88	203	203 (70), 119 (39), 83 (55), 56 (100)
D3	18.38	249	249 (6), 207 (20), 191 (63), 164 (41), 121 (100), 107 (15), 92 (16), 77 (17)
D4	12.53	220	220 (26), 192 (15), 121 (100), 107 (10), 92 (25), 77 (27)
D5	8.05	164	164 (62), 121 (81), 107 (57), 92 (100), 77 (20)
D6	9.92	164	164 (65), 150 (22), 121 (100), 107 (23), 92 (25), 77 (24)

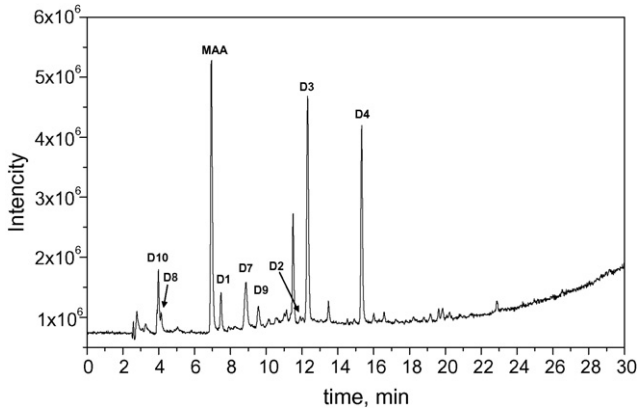

Fig. 5. LC/TOF-MS chromatogram, obtained after 15 min of TiO_2 treatment, where all the intermediates identified by LC–MS-TOF are present.

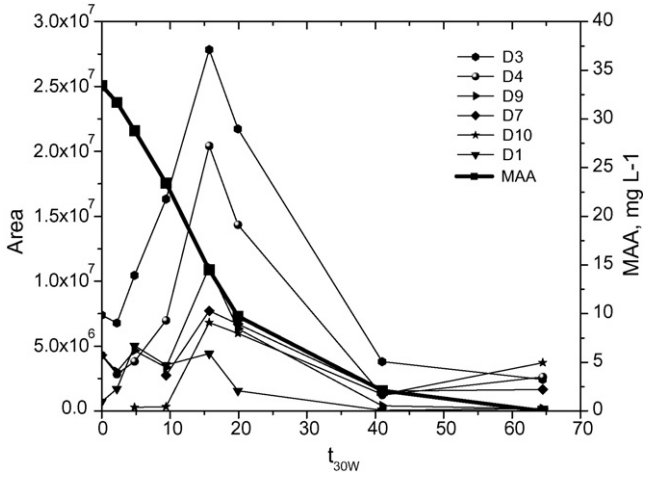

Fig. 6. Kinetics of the most important DPs formed during photocatalytic treatment.

been detected in groundwater, presumably from a nearby pharmaceutical plant [22].

4-Aminoantipyrin (D1) was the only DP detected by GC–MS that still conserves the heterocyclic ring. Its identity was also confirmed by the Wiley275 library with a 70% fit. The kinetics observed for this compound also support its identity since it appears early in the process and disappears while the open-ring derivatives are still present.

3.2.2. LC–TOF-MS analyses

By LC/TOF-MS, five additional intermediates were identified (D2, D7, D8, D9 and D10). Fig. 5 shows a LC/TOF-MS chromatogram obtained after 15 min of TiO_2 treatment, when all the compounds detected are present at their maximum intensity. Table 2 shows the measured and calculated mass of the protonated ions, the error between them and the proposed empirical formula corresponding to the compounds identified.

Very good concordance agreement between the experimental accurate mass measurements and the proposed formula (< 2.8 ppm error) was obtained in all cases. Proposal of chemical structures was possible were proposed based on the knowledge of the precursor molecule and the oxidative processes. A compound with the formula $C_{12}H_{16}N_3O_2$ corresponds to the addition of one oxygen atom to the MAA structure. This is consistent with the formation of a hydroxylated derivative, consequence of the addition of $^{\bullet}OH$ radicals to the aromatic ring, as is proposed in Fig. 3 (compound D8). Further oxidation of D8 yielded the corresponding quinone-imine intermediate (D9). Observation of double-bond equivalency (DBE) data, which represent on the number of rings and double bonds present in the molecule, is consistent with the proposed structures (see Table 2). The formation of compound D3 gave rise to the appearance of a series of derivatives after successive losses in the aliphatic chains (D4, D5, D6 and D7). Identification of D3 was confirmed by the presence of characteristic fragments at *m/z* 165 and 208, also present in the GC–MS spectrum and corresponding to the $[M + \text{H-COCONHCH}_2]^+$ and $[M + \text{H-COCH}_2]^+$ ions. The empirical formula of both fragments was confirmed with −1.4 and −1.2 ppm error, respectively.

Finally, aniline (D10) was also identified. The observation of the kinetics of the main DPs (Fig. 6) show that the photocatalytic degradation of MAA takes place mainly throughout the oxidation and opening of the heterocyclic ring, as the aromatic ring is more stable and resistant to degradation.

The samples from the photo-Fenton treatment are similar, except the severe conditions make most of the compounds present at the beginning of the experiment disappeared immediately after peroxide addition.

The majority of intermediates detected by LC–MS-TOF contained nitrogen in their structure (ammonia kinetics are shown in Figs. 1 and 2). The information provided by IC reveals

Table 2
Accurate mass measurements obtained by LC/TOF-MS from the spectra of dipyrone protonated degradation products

	Compound Rt	Formula	Calculated mass (*m/z*)	Measured mass (*m/z*)	mDa Error	ppm Error	DBE
D10	4.0	C_6H_8N	94.0651	94.0652	0.07	0.8	3.5
D8	4.1	$C_{12}H_{16}N_3O_2$	234.1237	234.1236	−0.1	−0.4	6.5
MAA	6.9	$C_{12}H_{16}N_3O$	218.1287	218.1287	<0.1	−0.4	6.5
D1	7.5	$C_{11}H_{14}N_3O$	204.1131	204.1130	−0.1	−0.6	5.5
D7	8.9	$C_9H_{11}N_2O_3$	195.0764	195.0759	−0.5	−2.6	5.5
D9	9.6	$C_{12}H_{14}N_3O_2$	232.1080	232.1078	−0.2	−1.0	7.5
D2	12.0	$C_{11}H_{13}N_2O$	189.1022	189.1017	−0.5	−2.8	6.5
D3	12.3	$C_{12}H_{16}N_3O_3$	250.1186	250.1180	−0.6	−2.4	6.5
D4	15.3	$C_{11}H_{13}N_2O_3$	221.092	221.0918	−0.3	−1.2	6.5

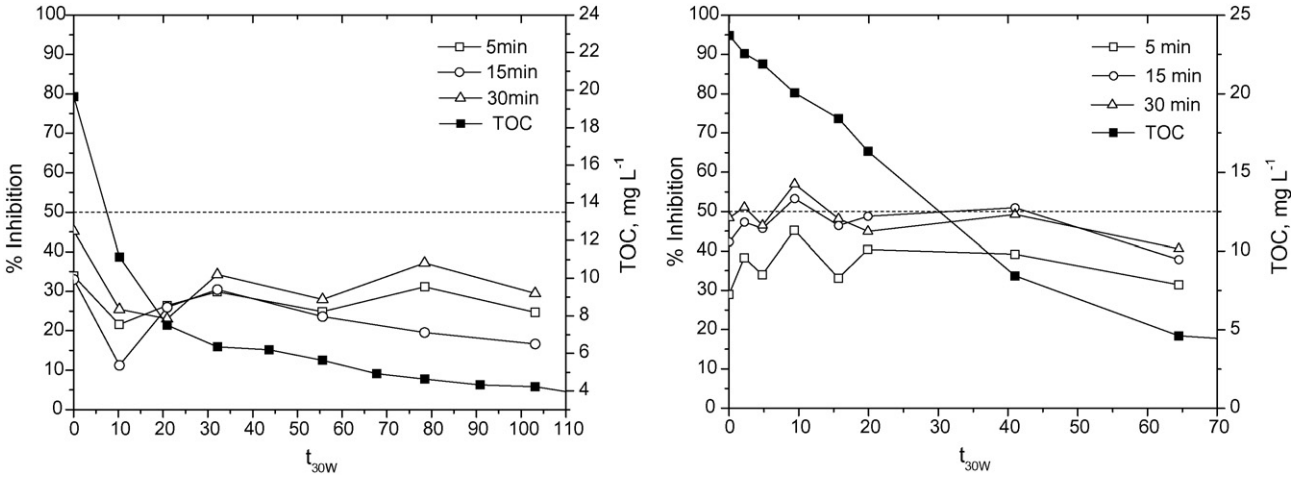

Fig. 7. Toxicity during photo-Fenton (left) and TiO_2 (right) treatments.

that nitrate is present at low concentrations during TiO_2 treatment, and ammonia is also negligible.

The MAA molecule contains a pyrazole structure, from which the (–NH–NH–) moiety releases N mainly in the form of N_2 (70% of the stoichiometric amount) and ammonia (approximately 7% of stoichiometric amount) [23,24]. During photo-Fenton treatment, ammonium was slowly released, but no significant quantities were found at the end of the treatment. The presence of aniline could be justified as the OH radical attack tends to occur preferably in the nitrogen atom instead of carbon. Therefore, the (–NH–C_6H_6) moiety is generally oxidized into aniline. This compound is present as one of the relevant ions, thus the proposed mechanism is congruent with the experimental data.

3.3. Toxicity evaluation

Toxicity was assessed in samples collected only after illuminating the photoreactor. Fig. 7 shows toxicity during both treatments. All the samples evaluated during the photo-Fenton treatment were below the 50% bioluminescent bacteria inhibition threshold. The slight toxicity detected (no more than 40% inhibition) could not be associated with MAA as it disappeared before the photo-Fenton reaction started (see Fig. 1). These results demonstrate that in photo-Fenton treatment solution toxicity does not increase due to the degradation products formed, as the treatment is sufficient to produce an effluent within a safe toxicity limits. Samples analyzed during the TiO_2 photocatalytic treatment showed a slight increase in toxicity during the first stages of the treatment, when the main degradation products generated are present at their higher concentration (Fig. 6). This increase is only observed during the TiO_2 treatment due to its slower kinetics. It can be also observed that after 10 min of photo-Fenton and TiO_2 treatment, the TOC measured was around 11 and 20 mg L^{-1}, respectively. When TOC was low enough during TiO_2 treatment, toxicity was similar to the photo-Fenton treatment. It could be mentioned that during TiO_2 treatment toxicity remained over the 50% threshold, while the MAA concentration was significant ($t_{30\ W} < 40$ min, MAA > 2.5 mg L^{-1}, see Fig. 2). Indeed, when only MAA was present at $t = 0$, toxicity was already at the 50% threshold. It may therefore be concluded that MAA is a matter of concern when discharged into the environment.

4. Conclusions

Photo-Fenton at very low iron concentration (Fe = 2 mg L^{-1}) is a quicker method of treating this type of compound with a pyrazole ring moiety than TiO_2 photocatalysis. Solar photo-Fenton provides a way to polish off the effluent of sewage treatment plants without removing iron after the treatment. In any case, this work also underlines the need for complete evaluation of AOP behaviour, not only by measuring the mineralisation of contaminants but also finding the main degradation intermediates and toxicity.

GC/MS analyses led to the identification of five DPs and analyses by LC/TOF-MS yielded the identification of five additional compounds, leading to a proposed degradation pathway yielding aniline as the main DP prior to opening of the ring. Toxicity assessment has demonstrated that MAA, the DP of major environmental concern, is degraded by both solar AOPs allowing safe disposal of the effluent.

Acknowledgements

The authors acknowledge the Spanish Ministry of Education and Science (Projects No CTM2004-06265-C03-03 and Programa Consolider Ingenio 2010 CE-CSD2006-004).

References

[1] S. Wiegel, A. Aulinger, R. Brockmeyer, H. Harms, J. Löffler, H. Reincke, R. Schmidt, B. Stachel, W. von Tümpling, A. Wanke, Chemosphere 57 (2004) 107.
[2] M.J. Gomez, M.J. Martínez Bueno, S. Lacorte, A. Fernández-Alba, A. Agüera, Chemosphere 66 (2007) 993.
[3] V. Koutsouba, Th. Heberer, B. Fuhrmann, K. Schmidt-Baumler, D. Tsipi, A. Hiskia, Chemosphere 51 (2003) 69.
[4] T. Heberer, Toxicol. Lett. 131 (2002) 5.
[5] T.A. Ternes, Water Res. 32 (1998) 3245.
[6] X.S. Miao, B.G. Koenig, C.D. Metcalfe, J. Chromatogr. A 952 (2002) 139.

[7] S. Ollers, H.P. Singer, P. Fasser, R. Muller, J. Chromatogr. A 911 (2001) 225.
[8] T.A. Ternes, Trends Anal. Chem. 20 (2001) 419.
[9] H. Ergün, D.A.C. Frattarelli, J.V. Aranda, J. Pharm. Biomed. Anal. 35 (2004) 479.
[10] Z. Moldovan, Chemosphere 64 (2006) 1808.
[11] C. Minero, E. Pelizzetti, S. Malato, J. Blanco, Chemosphere 256 (1993) 2103.
[12] D. Bahnemann, Solar Energy 77 (2004) 445.
[13] S. Malato, J. Blanco, A. Vidal, C. Richter, Appl. Catal. B: Environ. 37 (2002) 1.
[14] V. Augugliaro, E. Garcia-Lopez, V. Loddo, S. Malato-Rodriguez, M.I. Maldonado, G. Marcì, R. Molinari, L. Palmisano, Solar Energy 79 (2005) 402.
[15] L.A. Pérez-Estrada, S. Malato, W. Gernjak, A. Agüera, E.M. Thurman, I. Ferrer, A.R. Fernández-Alba, Environ. Sci. Technol. 39 (2005) 8300.
[16] C. Reyes, J. Fernández, J. Freer, M.A. Mondaca, C. Zaror, S. Malato, H.D. Mansilla, J. Photochem. Photobiol. A: Chem. 184 (2006) 141.
[17] L.A. Perez-Estrada, S. Malato, A. Agüera, A.R. Fernandez-Alba, in: D. Matazavinos, I. Poullos (Eds.), 1st Environmental Applications of Advanced Oxidation Processes, E-Proceedings, September 7–9, 2006.
[18] S. Malato, J. Blanco, A. Vidal, D. Alarcon, M.I. Maldonado, J. Cáceres, W. Gernjak, Solar Energy 75 (2003) 329.
[19] J. Pignatello, E. Oliveros, A. MacKay, Crit. Rev. Environ. Sci. Technol. 36 (2006) 1.
[20] V. Kavitha, K. Palanivelu, Chemosphere 55 (2004) 1235.
[21] J.C. Wessel, M. Matyja, M. Neugebauer, H. Kiefer, T. Daldrup, F.A. Tarbah, H. Weber, Eur. J. Pharm. Sci. 28 (2006) 15.
[22] K. Reddersen, T. Heberer, U. Dünnbier, Chemosphere 49 (2002) 539.
[23] P. Calza, E. Pelizzetti, C. Minero, J. Appl. Electrochem. 35 (2005) 665.
[24] K. Waki, J. Zhao, S. Horikoshi, N. Watanabe, H. Hidaka, Chemosphere 41 (2000) 337.